



ELSEVIER

Diamond and Related Materials 10 (2001) 132–138

**DIAMOND
AND
RELATED
MATERIALS**

www.elsevier.com/locate/diamond

Metal-containing amorphous carbon film development using electron cyclotron resonance CVD

Rusli^a, S.F. Yoon^{a,*}, Q.F. Huang^a, J. Ahn^a, Q. Zhang^a, H. Yang^a, Y.S. Wu^a, E.J. Teo^b, T. Osipowicz^b, F. Watt^b

^aSchool of Electrical and Electronic Engineering, Nanyang Technological University, Nanyang Avenue, Singapore 639798, Singapore

^bResearch Centre for Nuclear Microscope, Physics Department, National University of Singapore, 10 Kent Ridge Crescent, Singapore 119260, Singapore

Abstract

A technique for depositing metal–carbon (Me-C:H) thin films is demonstrated based on two metal screen grids embedded within an electron cyclotron resonance chemical vapour deposition (ECR-CVD) system. The grids are negatively biased and supported at adjustable distances above the substrate holder in the deposition chamber. With source gases of methane and argon, sputtering of the metal grids by Ar⁺ results in the incorporation of metal in the growing carbon films. The amount of metal in the films can be very well controlled over a wide range by varying the bias voltage at the grids, the separation of the grids from the substrate holder and the ratio of CH₄/Ar. Furthermore, by separately biasing the substrate holder, the properties of the films can be varied resulting in the formation of a great variety of Me-C:H films with very different mechanical and structural properties. Tungsten (W-C:H) and molybdenum (Mo-C:H) incorporated carbon films were deposited using this technique, with the metal fractions controlled by varying the flow ratio of CH₄/Ar and the bias at the substrates. The films were characterised using Rutherford backscattering, X-ray diffraction and Raman scattering measurements, and also in terms of their conductivity, optical absorption and hardness. Large changes are observed in the conductivity and optical gap of the films even at low fraction of metal incorporated. Metal carbides formation was observed for films deposited under bias. The results suggest that the substrate bias has a crucial effect on the incorporation of metal into the a-C:H films and their resulting microstructures. © 2001 Elsevier Science B.V. All rights reserved.

Keywords: Optical; DLC; Electrical; CVD

1. Introduction

Metal incorporated carbon (Me-C:H) films with properties intermediate between diamond-like carbon (DLC) and metal carbides have been shown to have small frictional values, extremely low abrasive wear rates and good adhesion to metal substrates [1,2]. Several techniques have been proposed for the deposition of Me-C:H films, which include sputter deposition in a hydrocarbon and Ar gas mixture [3], rf magnetron

sputtering [4], plasma polymerisation of a volatile metal organic compound [5], energetic metal ion implantation [6], co-evaporation of polymer and metal [7], co-sputtering of polymer and metal [8] and recently by magnetron assisted pulsed laser deposition [9]. Me-C:H films incorporated with different types of metal, such as Ta, Ti, Fe and W [3–6,9], have been studied in terms of their tribological and microstructural properties. In comparison, other important characteristics such as optical absorption and electrical conductivities of Me-C:H have not been widely investigated [2].

In the present work, we demonstrate a technique for depositing Me-C:H films based on an electron cyclotron resonance chemical vapour deposition (ECR-

* Corresponding author. Tel.: +65-7905428.

E-mail address: esfyoong@ntu.edu.sg (S.F. Yoon).

CVD) system in conjunction with a metal screen grid fixture situated within the deposition chamber. Using source gases of CH_4 and Ar, and with the metal grids under strong negative bias, the sputtering of the grids by Ar^+ can lead to the incorporation of the grid metal into the growing films. In this technique, the applied bias at the grid, the heights of the grids from the substrate holder and the flow ratio of CH_4/Ar can be varied to control the fraction of metal incorporated in the films. Through biasing the substrate, the energy of the impinging hydrocarbon ions can also be controlled. The uniqueness of this technique includes the high degree of ionisation in the ECR plasma, and also the ability to independently control the ionisation of the gases by the microwave power and the energy of the ions through the substrate bias.

W-C:H and Mo-C:H films were deposited using the above technique with two pure W or Mo grids in a gas mixture of CH_4 and Ar. The gas flow ratio and the dc bias applied at the substrates were varied to control the metal fraction in the films. These films were characterised in terms of their conductivity, hardness and atomic concentration by Rutherford backscattering (RBS) technique and structure by X-ray diffraction and Raman scattering measurements. The optical gap, which is seldom reported for Me-C:H films, was also investigated.

2. Experimental procedure

The details of the ECR-CVD system can be found elsewhere [10]. The ECR-CVD system has a downstream design whereby ions produced in the excitation chamber are extracted into the deposition chamber through the diverging magnetic field. The microwave power is introduced into the ECR magnetron excitation chamber through a quartz window. A magnetic field of 875 G required for the ECR condition is generated in the middle of the excitation chamber using the surrounding electromagnets. The substrates are located in the deposition chamber, placed onto a stainless steel plate that also forms the base of the screen grid fixture. The grid fixture is placed on top of a circular graphite receiver with a quartz plate placed in between for electrical isolation. Four poles made of insulating Vespal are used to position the lower and upper screen grid wire mesh. These grids are shorted together to a negative dc voltage of -330 V and the microwave power used was fixed at 400 W. Prior to deposition, the system was evacuated to below 5×10^{-6} torr using a turbomolecular pump. No intentional heating was applied during the depositions, and no appreciable increase in temperature was detected at the end of the deposition process. The substrates used consist of glass and (100)-oriented single crystal silicon.

3. Results and discussion

3.1. Tungsten-containing films

W-C:H films were deposited with square W meshes which have spacing between the wires of approximately 10 mm. The distance between the upper and lower screen grid was fixed at 5 cm, and the distance between the lower grid and the sample holder was fixed at 1.5 cm. The flow ratio of CH_4 to Ar was varied from 0.1 to 0.5 and the process pressure was maintained constant at 6 mTorr. Two series of films were grown, one with the substrates under floating condition with no bias applied and the other with a dc bias of -50 V applied. The W atomic fraction for the floating samples obtained using RBS increases from approximately 2% to approximately 8% as the flow ratio of CH_4/Ar decreases. The hardness of these films was measured using the Nanoindenter II system. The biased samples have hardness of approximately 10 GPa, compared to the floating samples of approximately 5 GPa. The hardness of both sets of films is found to be insensitive to the CH_4/Ar flow ratio, and hence the W contents. This may be due to the low W content in these films such that their mechanical properties are still predominantly controlled by the a-C:H matrix, which in turn is determined by the impinging ion energy, just as in the case of pure a-C:H films. XPS and XRD analysis of the floating samples showed no presence of WC bonds. In contrast, WC signals can be clearly seen for the biased samples. Fig. 1 shows the X-ray diffraction (XRD) spectra for the biased samples deposited at the two lowest CH_4/Ar ratios of 0.1 and 0.2, measured using the Siemens D5005 X-ray diffractometer with Cu K_α radiation ($\lambda = 1.54 \text{ \AA}$). The size of the WC nanocrystals, estimated using the WC (111) peak seen in the XRD spectra and based on the Debye–Scherrer formula, is approximately 2.3 nm. The results suggest that certain minimum amount of ion energy is required for the formation WC in these films.

Fig. 2 shows the resistivity of the films measured using the four-point probe technique for both the floating and biased samples. There is a drastic drop in the resistivity of the samples at decreasing CH_4/Ar ratio, attributed to the incorporation of W in the films. It is noted that in the case of biased substrates, the change in resistivity spans almost nine orders of magnitude. In the regime of higher CH_4/Ar ratio (lower W content), the biased samples have resistivities in the range of $10^7 \text{ } \Omega \text{ cm}$, typical of pure a-C:H films. Except at lower CH_4/Ar ratio, the biased samples consistently have larger resistivity compared to the floating samples. Besides being related to the amount of W incorporation in the films, the different in the microstructures of these films deposited under different bias conditions could also account for the results observed. The biased

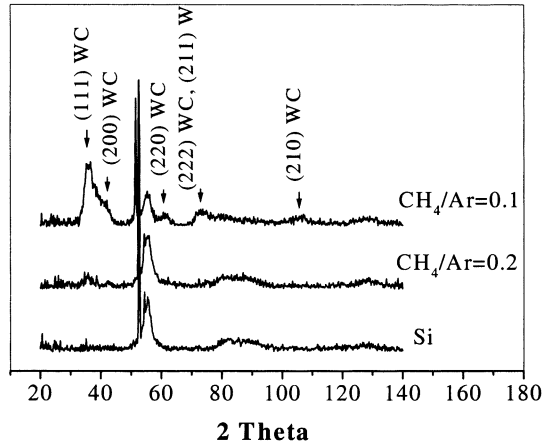


Fig. 1. XRD patterns from the biased W-C:H samples with larger W contents, at the lowest CH_4/Ar flow ratios of 0.1 and 0.2.

samples are expected to be more constrained due to their denser and more cross-linked network, as can be induced from their higher hardness, which could discourage the incorporation of W atoms in the case of lower W fraction. However, at higher W fraction (smaller CH_4/Ar ratio) when the W clusters dominate the conduction behaviour, it was found that both the biased and floating samples exhibit similar resistivities with respect to the CH_4/Ar gas flow ratio.

Fig. 3a shows the conductivity of the biased samples measured at different temperatures. The conductivity was modelled in the simplest form, $\sigma = \sigma_0 \exp(-E_a/kT)$, assuming temperature independent prefactor σ_0 and activation energy E_a . Reasonable fits (solid lines in Fig. 3a) are obtained for the samples over the temperature range studied. Our modelling serves only to provide a measure of the degree of thermal activation in the conductivity, rather than implying any prevailing conduction behaviour in these films, as there

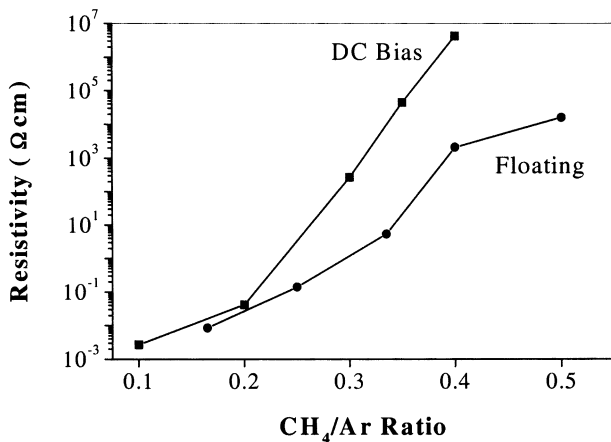


Fig. 2. The resistivity of the W-C:H films measured using the four-point probe technique at different CH_4/Ar ratios for the biased (-50 V dc) and floating samples.

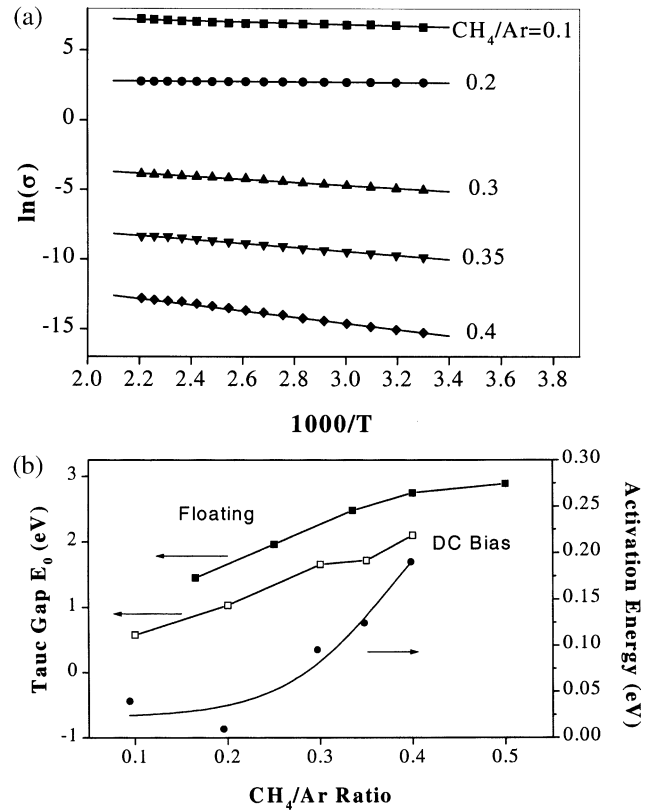


Fig. 3. (a) The conductivity of the biased W-C:H samples measured as a function of temperature (b). Activation energy for the biased W-C:H samples and the Tauc gap (E_0) for both sets of films at different CH_4/Ar flow ratios.

exists no well-established conduction model for these Me-C:H films to date. It should be noted that recently we have attempted to model the conduction behaviour of Me-C:H films in detail [11]. Fig. 3b shows the activation energy E_a of the biased samples. The results reveal thermally activated process for all the samples, with the activation energy decreases at increasing W content. Activation energy measurements were similarly performed for the floating samples, however, over a narrower temperature range from room temperature to 150°C due to these samples being thermally less stable. A much steeper increase in the conductivity with temperature was clearly observed for films with lower W fractions, similar to the case of the biased samples. The observed thermally activated conduction behaviour could be attributed to the tunnelling of electrons between the metal clusters, with the decrease in activation energy at higher W content indicating the transition of these films from semiconductor-like to metallic-like [12].

The optical absorption in these films are obtained using samples deposited on glass substrates, through their transmittance and reflectance measured by a Perkin-Elmer Lambda 16 dual beam spectrophotometer. Fig. 3b shows the Tauc gaps (E_0) for both sets of

films as a function of the CH_4/Ar ratio. Both the optical gaps decrease sharply by more than 1.5 eV over the range of CH_4/Ar ratio studied, which is certainly related to the increased absorption in the presence of W clusters. The floating samples also consistently exhibit higher optical gaps than the biased samples, which could be related to their more polymeric structure, and is consistent with the hardness results. It should be noted that the large variation in the optical gap is strongly correlated to the drastic decrease observed in the resistivities of these films.

3.2. Molybdenum-containing films

Commercially acquired high purity Mo grids measured $100\text{ mm} \times 100\text{ mm}$, having wire diameter of 0.18 mm and spacing between the wires of 0.8 mm were used for the deposition. The distance between the upper and lower screen grid, and between the lower grid and the sample holder were fixed at 2.8 cm. The rf power was varied from 0 W to 125 W resulting in self-induced dc bias voltages over a range of -38 V to -130 V . The process pressure was maintained constant at 8 mTorr and the CH_4/Ar flow ratio was fixed at 15/20 sccm.

Rutherford backscattering (RBS) and particle induced X-ray emission (PIXE) spectra confirmed the presence of Ar, Mo and Si (substrate) in these films. The RBS spectra of the samples deposited at -115 V , -105 V and -90 V revealed a two-layer structure with different fractions of Mo incorporated in each layer. Table 1 shows the atomic fraction of Mo, O and Ar relative to carbon for all the films, deduced from RBS measurements. For the samples with a two-layer structure, layer 1 refers to the top layer whereas layer 2 refers to the layer next to the substrate. The average Mo/C fractions for these samples taking into account the thickness of the individual layers are also shown. In the thickness calculation, the atomic densities of the films used are estimated from the average of the densities of the constituent elements, weighted by the composition ratio. This, coupled with the fact that we have ignored the H content in the samples, will result in some errors and hence the thickness shown may not represent the true thickness of the films. It is noted that there is an increase in the average Mo fraction at larger dc bias voltages, except for the sample deposited at the lowest bias voltage. This increase in the Mo fraction in the films at larger bias can be attributed to the presence of Mo^+ ions being created by the energetic electrons in the ECR plasma. At increasing negative bias voltage, the Mo^+ ions are strongly accelerated towards the substrate, leading to a larger fraction of Mo being incorporated into the films. The Mo^+ ions are also expected to play a significant role, in addition to the Ar^+ ions, in modifying the structures of these

Table 1

The relative atomic fractions of Mo, O and Ar with respect to C deduced using RBS for films deposited at different bias voltages^a

RF-induced DC Bias (V)	Layer	Thickness (nm) ^b	Mo	Mo (average)	O	Ar
-130	1	84.3	0.0393	-	0.15	-
-115	1	114.0	0.0223	0.0320	0.006	0.0021
	2	39.6	0.0624		0.006	0.0022
-105	1	96.2	0.0121	0.0194	0.006	0.002
	2	54.1	0.0334		0.006	0.0021
-90	1	79.8	0.00818	0.0132	0.005	0.0066
	2	38.7	0.0239		0.005	0.0062
-65	1	68.9	0.0128	-	0.145	-
-38	1	36.2	0.0229	-	0.18	-

^aFor samples that were fitted as a two-layer system, layer 1 refers to the top layer whereas layer 2 refers to the layer underneath, next to the substrate.

^bThe data given have ignored the content of H in the samples. The thickness given may therefore not represent the true thickness of the films.

films through energetic bombardment at the surface of the growing films. This effect can be significant due to the large mass of the Mo^+ .

Fig. 4 shows the X-ray diffraction (XRD) pattern for the Mo-C:H film deposited at the highest dc bias of -130 V . Besides the crystalline Si substrate peaks, other diffraction peaks corresponding to crystalline MoC(205), $\text{Mo}_2\text{C}(102)$ and Mo(211) were noted. The spectrum is typical of those obtained for the other samples and indicates the presence of MoC crystallites in the films. Fig. 5a shows the resistivity of the films measured using the four-point probe technique. A sharp decrease in the resistivity seen at increasing dc bias voltage is clearly related to the increase in the Mo fraction in the films. Two plateau regions in the variation of the resistivity with dc bias are observed: one at the lower bias range and the other at the higher bias range. From Table 1, it can be seen that at the lower bias voltages of -38 V and -65 V , Mo appears close to the film surface. As the bias voltage is increased to -90 V , the surface O and Mo fractions are observed to decrease, possibly due to enhanced sputtering at larger bias voltage. Mo is detected approximately 80 nm below the film surface. The oxygen contents of these films deposited at intermediate bias voltages are relatively low compared to those grown at substrate bias of -38 V , -65 V and -130 V . The slow increase in average Mo from 0.0132 to 0.032 cannot account for the drastic drop of nine orders of magnitude in resistivity for films grown at -90 V , -105 V and -115 V . The decrease in resistivity for these films could be

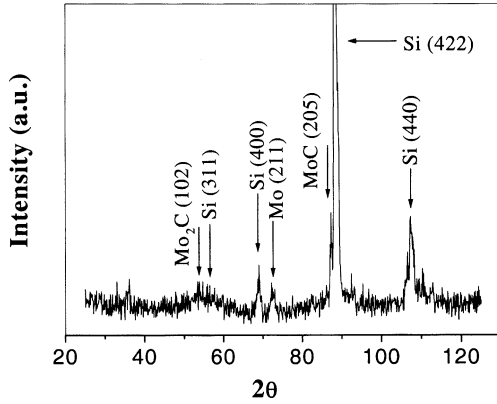


Fig. 4. XRD pattern for the Mo-C:H film deposited at dc bias voltage of -130 V.

linked to microstructural transition in the films. The impinging Mo ions could be energetic enough to be implanted into the deeper layer of the films as the substrate bias voltage is increased. This can result in the formation of large Mo clusters for a Mo/C fraction of 0.0624 as indicated in Table 1 (or 5.8 at.% Mo), at approximately 114 nm below film surface for the sample deposited at -115 V. At -130 V, the resistivity of the film reaches a plateau, and the oxygen content increases to approximately 15%. New species of Mo oxides instead of Mo clusters could have formed at the high bias voltage.

The conductivity of the films was also studied over a temperature range from 303 K to 450 K with the results shown in Fig. 5b. Higher temperature measurements were not carried out to avoid structural changes that can be caused by increased oxidation (metal-oxide) in these films, dehydrogenation and graphitisation of the hydrocarbon matrix. As in the case of W-C:H films, the conductivity was modelled in the simplest form $\sigma = \sigma_0 \exp(-E_a/kT)$. The fittings are shown by the solid lines in Fig. 5b, and the activation energies deduced are shown in Fig. 5a. It can be seen that the simple model reasonably describes the data for all the samples over the range of temperature studied. The activation energy results reveal a thermally activated conductivity for samples with low Mo fraction. A decrease in the dependence of the conductivity on temperature at higher Mo fraction suggests an enhanced metallic conduction in these films, similar to the case of W-C:H films.

Tauc gaps (E_0) deduced for these films deposited on glass substrates are shown in Fig. 6. The optical data were determined assuming a single layer optical model, ignoring the two-layer structure found in three of the samples. This should not critically affect the trend observed for E_0 given the large change in the optical gap in these films. The sharp drop in E_0 at increasing dc bias voltage is closely related to the increased in the

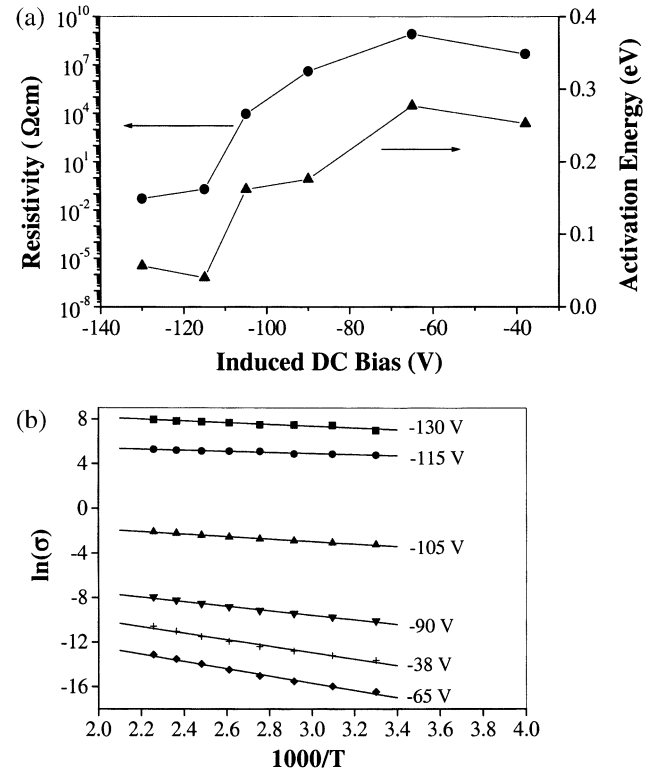


Fig. 5. (a) Resistivity measured using the four-point probe technique and the activation energy of the Mo-C:H films deposited at different bias voltages. (b) Conductivity of the Mo-C:H films measured as a function of temperature.

Mo fractions in the films. Similar to the case of W-C:H films, there is a strong correlation between the electrical and optical properties of these films, and similar sharp transition in these properties can be observed over the dc bias range from -105 V to -115 V.

The hardness of the films are shown in Fig. 6, where decreasing hardness can be seen at increasing dc bias. For the case of W-C:H films, it was found that the mechanical properties of the films were mainly controlled by the a-C:H matrix at lower W fraction. A

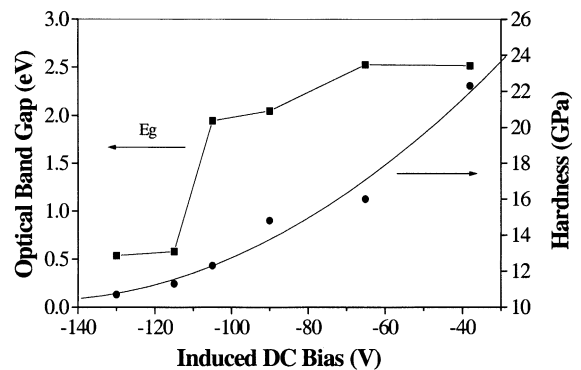


Fig. 6. The Tauc gap and hardness of the Mo-C:H films deposited at different bias voltages.

similar conclusion was derived for another series of Mo-C:H films deposited at constant substrate bias. However, the films exhibited increased hardness once the Mo fraction exceeded certain threshold value, attributed to the formation of Mo carbides in these films [13]. The low level of Mo fraction in this series of Mo-C:H films should also not influence the film hardness. The reduced hardness for films with larger Mo fraction deposited at larger bias voltages can be attributed to energetic ion bombardment that amorphises the films and promotes the growth of sp^2 bonded carbon. The proposed structural change is supported by the Raman scattering results shown in Fig. 7, which was excited with an Ar^+ laser at 514.5 nm and measured using a SPEX1400 system. It can be seen that there is an increase in the intensity of the D peak (approx. 1367 cm^{-1}), attributed to the disorder activated optical zone-edge phonons, relative to that of the G peak. This increase has been previously correlated to an increase in the sp^2/sp^3 bonded carbon in DLC films [14]. Assuming that the Raman scattering of the Mo-C:H films are derived mainly from the hydrocarbon matrix given the low Mo fractions, the increase in the sp^2 fraction in the films at higher Mo fraction can therefore account for the decreased hardness observed. The increase in the carbon sp^2/sp^3 ratio as seen from the Raman results, could have also affected the resistivity of these films [15]. Their contribution is expected to be significant when the atomic fraction of metal involved in small.

In our experiment, it was also noted that samples deposited on glass generally tend to contain slightly larger metal fractions, as deduced from their more metallic appearance, particularly for films with higher levels of Mo. Since the conductivity was measured using the four-point probe technique for films deposited on glass substrates, whereas the atomic frac-

tions were determined by RBS for films deposited on Si substrates, therefore the large conductivity observed at the relatively low level of Mo incorporated for these films could also be partly attributed to the different substrates used for the measurement.

4. Conclusion

From the thermally activated conduction behaviour, it can be deduced that electrical conduction in these films occurs mainly through the tunnelling of electrons between metal clusters, which are embedded within an amorphous carbon matrix. Since the metal fractions in all these samples are less than 10%, it is believed that the metal clusters do not yet form a continuous network. The mechanical properties of the films are predominantly determined by the microstructures of the amorphous hydrocarbon network, which in turn are determined by the energy of the impinging ions through the applied bias at the substrates. The drastic decrease in the resistivities of these films could also be attributed to the microstructural changes, in terms of the fraction of sp^2/sp^3 bonded carbon, as a result of energetic ion bombardment.

It should be mentioned that the presence of oxide in these films could have some impact on their mechanical and electrical properties. These films are sensitive to oxygen, which could react to form metal oxide either during the deposition and/or upon post-deposition. Our recent XPS depth profiling measurement on Mo-C:H films revealed a high concentration of oxygen at the surface of these films, which consequently decreased towards the bulk of the films [16]. This observation suggests that post-oxidation could be significant. It is believed that similar behaviour also occurs in W-C:H films due to the high reactivity of the metal. The presence of oxygen could affect the electrical properties measured as most of oxygen atoms are located near the surface. It is believed that the conductivity of the films will decrease as a result, especially for those incorporated with a high fraction of metal fractions.

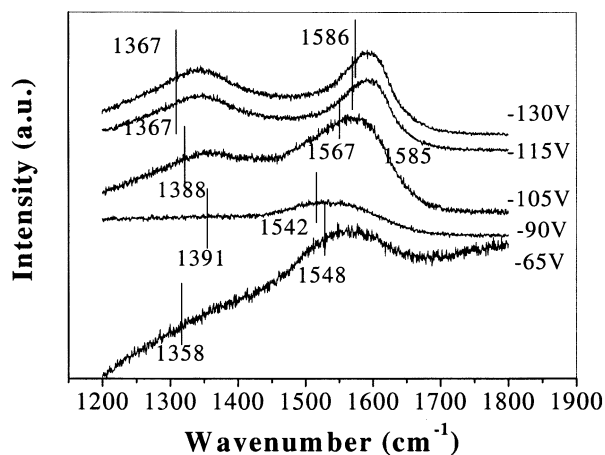


Fig. 7. Raman scattering spectra of the Mo-C:H films deposited at different bias voltages.

References

- [1] H. Dimigen, H. Hubsch, R. Memming, *Appl. Phys. Lett.* 50 (1987) 1056.
- [2] C.P. Klages, R. Memming, *Mater. Sci. Forum* 52/53 (1989) 609.
- [3] C. Benndorf, M. Grischke, H. Koeberle, R. Memming, A. Brauer, F. Thieme, *Surf. Coat. Technol.* 36 (1988) 171.
- [4] P.K. Srivastava, T.V. Rao, V.D. Vankar, K.L. Chopra, *J. Vac. Sci. Technol. A* 2 (1984) 1261.

- [5] C. Benndorf, J.T. Harnack, U. Fell, *Surf. Coat. Technol.* 59 (1993) 345.
- [6] T.M. Wang, W.J. Wang, C. Jing, *Diamond Relat. Mater.* 5 (1996) 1418.
- [7] S.A.Y. Al-Ismail, C.A. Hogarth, *J. Mater. Sci.* 22 (1987) 415.
- [8] R.A. Roy, R. Messier, J.M. Cowley, *Thin Solid Films* 79 (1981) 207.
- [9] A.A. Voevodin, M.A. Capano, A.J. Safriet, M.S. Donley, J.S. Zabinski, *Appl. Phys. Lett.* 69 (1996) 188.
- [10] S.F. Yoon, Rusli, J. Ahn, Q. Zhang, Y.S. Wu, H. Yang, *J. Vac. Sci. Technol A* 17 (1999) 121.
- [11] Q.F. Huang, S.F. Yoon, Rusli, H. Yang, B. Gan, K. Chew, J. Ahn, *J. Appl. Phys.* 88 (2000) 4191.
- [12] H. Koeberle, M. Grischke, F. Thieme, C. Benndorf, R. Memming, *Surf. Coat. Technol.* 39/40 (1989) 275.
- [13] Q.F. Huang, S.F. Yoon, Rusli, H. Yang, J. Ahn, Q. Zhang, *Diamond Relat. Mater.* 9 (2000) 534.
- [14] M. Yoshikawa, G. Katagiri, H. Ishida, A. Ishitani, *J. Appl. Phys.* 64 (1988) 6464.
- [15] H. Koeberle, M. Grischke, F. Thieme, C. Benndorf, R. Memming, *Surf. Coat. Technol.* 39/40 (1989) 275.
- [16] S.F. Yoon, Q.F. Huang, Rusli, H. Yang, J. Ahn, Q. Zhang, C. Blomfield, B. Tielsch, L.Y.C. Tan, *J. Appl. Phys.* 86 (1999) 4871.